Materials Research. 2019; 22(suppl. 2): e20180748
DOI: http://dx.doi.org/10.1590/1980-5373-MR-2018-0748

Microstructure and Properties of Duplex Ni-P-TiO_2/Ni-P Nanocomposite Coatings

***Weihui Zhang*[a], *Di Cao*[a], *Yanxin Qiao*[a], *Zhen He*[a], *Yuxin Wang*[a]*, *Xiang Li*[b], *Wei Gao*[c]**

[a]*School of Materials Science and Engineering, Jiangsu University of Science and Technology, Zhenjiang, 212003, Jiangsu, China*
[b]*School of Materials Science and Engineering, University of Shanghai for Science and Technology, Shanghai 200093, China*
[c]*Department of Chemical & Materials Engineering, the University of Auckland, PB 92019, Auckland 1142, New Zealand*

Received: November 22, 2018; Revised: February 15, 2019; Accepted: April 29, 2019

Duplex Ni-P-TiO_2/Ni-P coatings were electrodeposited onto brass substrates. High phosphorus Ni-P coatings were plated as the inner layer to improve the corrosion resistance, while low phosphorus sol-enhanced Ni-P-TiO_2 coatings were deposited on the top to strengthen the mechanical property. The microstructure, morphology, mechanical property and corrosion resistance of coatings were investigated systematically. The results show that duplex coatings exhibit both excellent mechanical property and good corrosion resistance. The hardness was further improved from ~545 HV_{50} of duplex Ni-P/Ni-P coating to ~622 HV_{50} of duplex Ni-P-12.5mL/L TiO_2/Ni-P coating, while the hardness of single Ni-P coating was only ~387 HV_{50}. The corrosion resistance of duplex coatings improved significantly by adding a suitable amount of TiO_2 sol. Duplex Ni-P-12.5mL/L TiO_2/Ni-P coating presented the highest corrosion resistance. However, adding excessive quantities of sol (more than 12.5mL/L) caused nanoparticle agglomeration and created a porous structure in the outer layer, deteriorating the properties of coatings.

Keywords: *Duplex coatings, sol-enhanced electrodeposition, Ni-P coating, corrosion resistance.*

1. Introduction

As one of the most widely used coatings in industry, Ni-P coatings have attracted great attention due to their unique properties, such as shinning surface, high wear resistance and excellent corrosion resistance [1-3]. In order to address more challenging applications, how to further increase the performance of Ni-P coatings has become a hot spot in current research.

It is well known that high P Ni-P coatings possess relative high corrosion resistance, while medium and low P containing coatings have relative high hardness [4,5]. As the microstructure and properties of Ni-P coatings are mainly dependent on the phosphorus content, fabricating duplex Ni-P coating system is an effective way to obtain both good mechanical properties and high corrosion resistance [6]. In the duplex Ni-P coating system, a high phosphorus Ni-P coating was usually deposited as the inner layer to protect the substrate matrix due to its excellent corrosion resistance. Different kinds of hard coatings such as Ni-B[7] and Ni-P[8] coatings were deposited as the outer layer in order to improve the mechanical properties.

In order to further improve the performance of outer layer coating, many research have been carried out by incorporating second phase nanoparticles [9-11] to synthesize duplex Ni-P nanocomposite coatings. However, it is hard to achieve a good suspension of nanoparticles in the coating matrix due to their small size and high surface energy, thus impeding the further development of coating performance. To avoid nanoparticles agglomeration, we recently developed a novel sol-enhanced plating method [12]. This method which combines the sol-gel process with electrodeposition can lead to a highly distribution of oxide nanoparticles in the coating matrix, resulting in significantly improved mechanical properties. Based on this new technology, electroless double-layered Ni-P-$XZrO_2$/Ni-P coatings with different phosphorus (P) contents have been prepared on stainless steel[13] and AZ31 magnesium alloy[14], respectively. These duplex coatings may find a promising industry applications as they exhibit excellent mechanical property and high corrosion resistance.

Comparing with Ni-P electroless plating which has a relatively complicated process and usually requires a high operating temperature, Ni-P electroplating is easy to operate and the deposition rate can be accurately controlled by adjusting plating current. In this paper, duplex Ni-P-TiO_2/Ni-P coatings were deposited on the brass substrate by electroplating method. High phosphorus Ni-P coating was plated as the inner layer to ensure good corrosion resistance, while low phosphorus sol-enhanced Ni-P-TiO_2 coating was deposited as the outer layer to strengthen the mechanical property. Different contents of phosphorus in the inner and outer layers were simply achieved by changing the phosphoric acid content. The microstructure, morphology, mechanical property and electrochemical property of coatings were systematically investigated.

*e-mail: ywan943@163.com

2. Experimental

2.1 Sample preparation

Duplex Ni-P-TiO_2/Ni-P coatings were electroplated onto the brass substrates (20×30×0.3mm^3). Before electroplating, the specimens were ultrasonically cleaned for 1min, alkali washed at 65 ºC for 5min in a solution containing 50g/L NaOH and 10g/L $NaH_2PO_4 \cdot H_2O$, then activated by a solution comprising 20g/L citric acid and 60g/L ammonium citrate for 1min at room temperature (about 25 ºC). Specimens were washed with distilled water between each steps. The bath composition and plating parameters of basic Ni-P coating are given in Table 1. The duplex Ni-P-TiO_2/Ni-P coatings were obtained by controlling the contents of phosphoric acid and TiO_2 sol in the basic Ni-P electrolyte, and the flow diagram of sample preparation is shown in Fig. 1. TiO_2 sol was prepared as reported in the previous papers [15-18]. For comparison purposes, a duplex Ni-P/Ni-P coating without adding sol was prepared with the identical plating parameters.

2.2 Sample characterization

The phase structure of the coatings was examined using an X-ray diffractometer (Bruker D2, Germany, V= 30 kV, I= 15 mA) with copper Kα radiation (λ= nm) under the scanning speed of 0.5º/min.

Field-emission scanning electron microscopy (FE-SEM, ZEISS Merlin Compact, Germany) equipped with an energy dispersive spectroscopy (EDS) system was used to examine the cross-section microstructure of the coatings. Confocal laser scanning microscopy (LEXTOL S4000, Olympus, Japan) was used to analyze the surface morphology of the coatings.

A Vickers microhardness tester was used to investigate the microhardness of the coatings. During the tests, an indentation load of 50 g with the loading time of 15 s were used. All the wear tests were performed under the load of 7 N with a sliding speed of 20 mm/s. The radius of sliding ball was 9.58 mm and the total sliding distance was 12m. The wear track width of coatings was observed by using optical microscope images.

The corrosion resistance of coatings was assessed by an electrochemical workstation (CS2350H). All the corrosion tests were performed at room temperature by using a classical three-electrode cell with a platinum (Pt) as the counter electrode, a Ag/AgCl electrode as the reference electrode and a coating specimen as the working electrode. The exposed area of specimens was set to 1cm^2. Prior to measurements, the samples were subjected to open circuit conditions for 30min until a steady-state potential was reached. The electrochemical impedance spectroscopy (EIS) measurements was measured in the frequency range from 1×10^5 Hz to 1×10^{-2} Hz with the applied AC amplitude of 10mV.

Table 1. Bath composition and electroplating parameters for basic Ni-P coating.

Bath constituents	Quantity	Conditions
$NiSO_4 \cdot 6H_2O$	250 g/L	PH: 3±0.5
$NiCl_2 \cdot 6H_2O$	15 g/L	Agitation speed: 300 rpm
NaCl	15 g/L	Temperature: 70±2ºC
H_3BO_3	30 g/L	Current density: 20 mA/cm^2
$NaH_2PO_2 \cdot 6H_2O$	20 g/L	
85% H_3PO_4	10 g/L for High P Ni-P coating	
	25 g/L for low P Ni-P coating	
TiO_2	0, 12.5 mL/L, 50 mL/L	

Plating time: (1)35 min for single high P Ni-P coating; (2)35 min for high P Ni-P inner coating, 35 min for low P Ni-P coating or sol-enhanced Ni-P-X mL/L TiO_2 outer coating (X=12.5, 50).

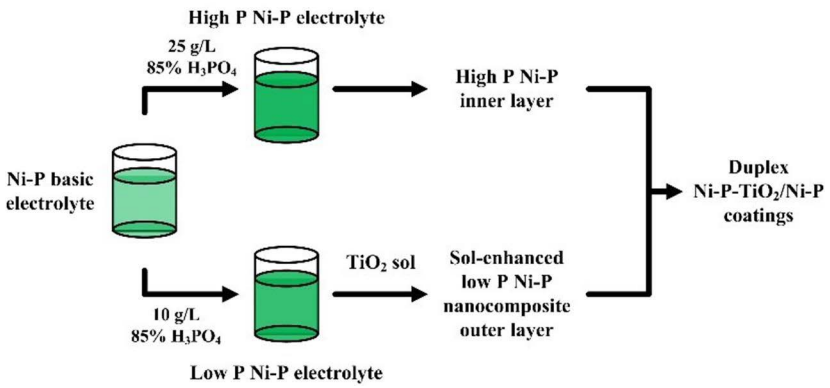

Figure 1. Operation flow chart of duplex coatings.

The impedance data were analyzed on the basis of equivalent electrical circuit using the Zsimpwin software. The potentiodynamic polarization tests were conducted at a scanning rate of 1mV/s in 3.5 wt.% NaCl solution.

3. Results and Discussion

3.1 Phase structure of coatings

The phase structures of single Ni-P coating and duplex Ni-P-TiO_2/Ni-P nanocomposite coatings are shown in Fig. 2. It can be seen that Ni (111) and brass phases exist in the diffraction curve of single high P Ni-P coating. After depositing low P Ni-P coating on the high P Ni-P layer, some diffraction peaks derived from the brass substrate could not be detected, which can be attributed to the increase of coating thickness. All the duplex coatings exhibit the similar diffraction patterns, showing that the addition of TiO_2 sol did not induce the variation of coating phase. No TiO_2 diffraction peaks could be detected from all duplex Ni-P-TiO_2/Ni-P nanocomposite coatings probably due to the low quantity of TiO_2 and high intensity of other diffraction peaks.

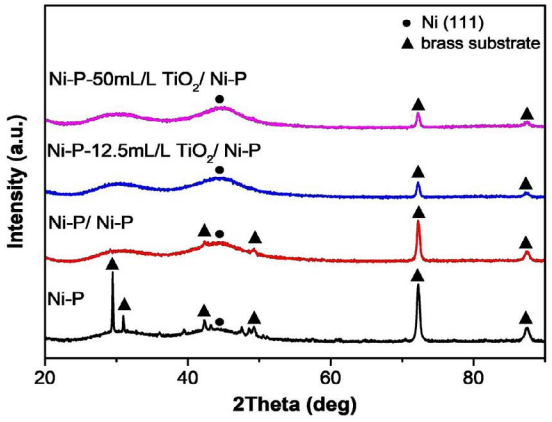

Figure 2. XRD patterns of single Ni-P coating and duplex Ni-P-TiO_2/Ni-P coatings.

3.2 Surface and cross-sectional morphologies of coatings

Fig. 3 presents the surface morphology of duplex Ni-P/Ni-P and duplex Ni-P-12.5mL/L TiO_2/Ni-P coatings. All coatings show a typical morphology of spherical shape. Duplex Ni-P/Ni-P coating has a relatively large grain size with an average diameter of ~3.8μm as shown in Fig. 3(a). As shown by the black arrows in the Fig. 3(b), there are many nanoparticles distributed around the grain boundary areas. The sol-enhanced duplex Ni-P-12.5mL/L TiO_2/Ni-P coating has a relatively smaller grain size with a mean size of ~2.1μm. The grain refinement of sol-enhanced duplex coating could be attributed to the highly dispersed TiO_2 nanoparticles. These incorporated TiO_2 nanoparticles distributed in the grain boundary areas can provide more nucleation sites and effectively hinder the grain growth, resulting in a smaller grain size.

The cross-sectional SEM images of coatings and a qualitative elemental distribution line scan are shown in Fig. 4. The single Ni-P coating has a total thickness of ~4 μm, indicating a deposition speed of ~ 7 μm/h. Duplex Ni-P/Ni-P coating has a total thickness of ~10 μm with ~4 μm inner layer and ~6 μm outer layer. The thickness of duplex Ni-P-TiO_2/Ni-P coatings was increased gradually following with the increasing TiO_2 addition. The thickness of Ni-P-12.5mL/L TiO_2/Ni-P coating and Ni-P-50mL/L TiO_2/Ni-P coating was gradually increased to ~11 μm and ~13.5 μm, respectively. The variation of coating thickness could be attributed to the incorporation of TiO_2 which can provide more nucleation sites. All the coating exhibits a good adhesion to the substrate as no defects or cracks could be observed at the interfaces. The interfaces between two layers are very uniform and clean, as shown in Fig. 4(b)-4(d). The low P Ni-P-TiO_2 outer layer of Ni-P-12.5mL/L TiO_2/Ni-P coating exhibited a homogeneous structure with some tiny visible TiO_2 nanoparticles agglomeration as depicted in Fig. 4(c).

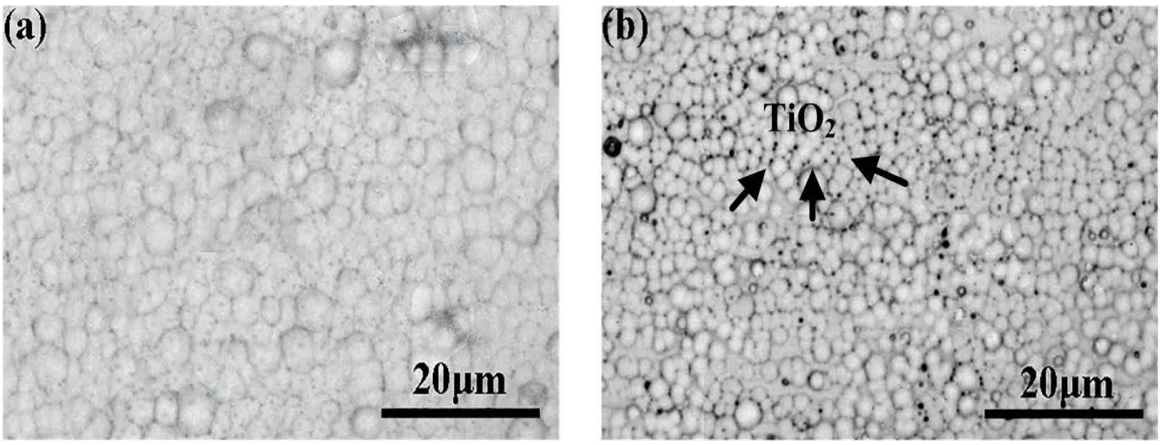

Figure 3. Surface morphology of duplex coatings: (a) duplex Ni-P/Ni-P coating, (b) duplex Ni-P-12.5mL/L TiO_2/Ni-P coating.

When increasing the sol addition to 50 mL/L, more agglomeration areas and even small voids can be clearly observed in the outer layer matrix. EDS results indicated that phosphorus content of outer layer was not influenced by sol doping. The phosphorus contents of low P and high P layers were ~8wt.% and ~11wt.%, respectively, based on the quantitative analysis of coating.

3.3 Mechanical property of coatings

3.3.1 Microhardness

Fig. 5 shows the microhardness of Ni-P coating and duplex Ni-P-TiO_2/Ni-P nanocomposite coatings. The microhardness of Ni-P/Ni-P coatings is ~545 HV_{50},

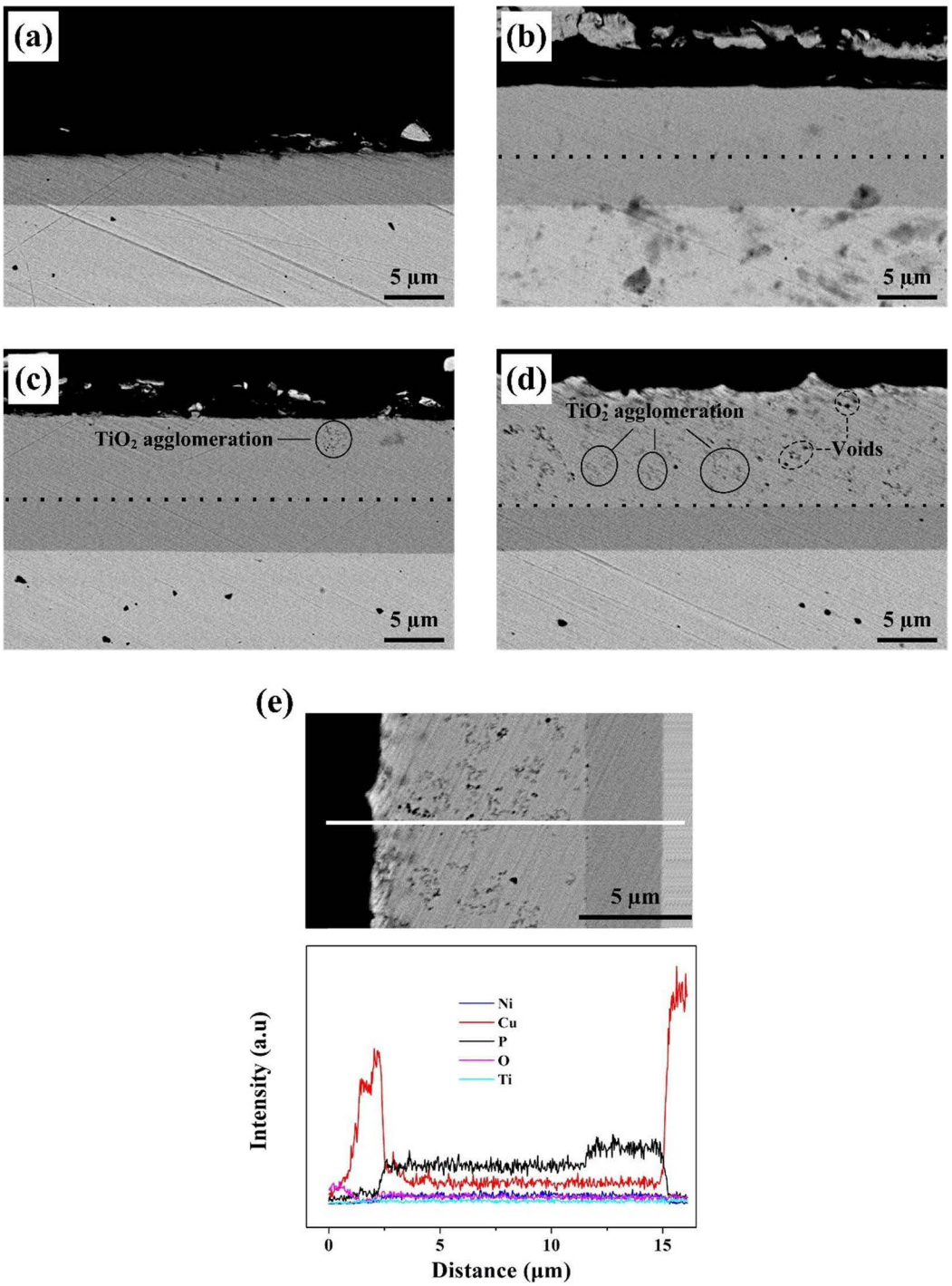

Figure 4. Cross-sectional image of (a) single Ni-P coating, (b) duplex Ni-P/Ni-P coating, (c) duplex Ni-P-12.5mL/L TiO_2/Ni-P coating and (d) duplex Ni-P-50mL/L TiO_2/Ni-P coating, and line scan of (e) duplex Ni-P-50mL/L TiO_2/Ni-P coating.

which increased nearly 41% compared with ~387 HV_{50} of single Ni-P coating. The improvement of coating hardness can be attributed to the variation of P contents in the coating and the increase of coating thickness.

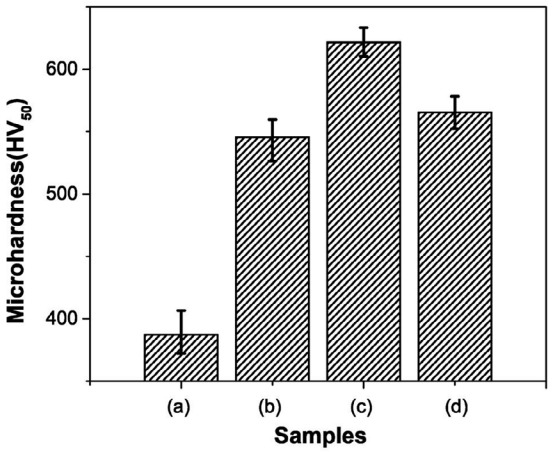

Figure 5. Microhardness of (a) Ni-P; (b) Ni-P/Ni-P; (c) Ni-P-12.5mL/L TiO_2/Ni-P; (d) Ni-P-50mL/L TiO_2/Ni-P.

When proper TiO_2 sol was added into the electrolyte, the microhardness of duplex coatings enhanced significantly. The microhardness of Ni-P-12.5 mL/L TiO_2/Ni-P coating reached to a relatively high value of ~622 HV_{50}. Correspondingly, when excessive TiO_2 sol was added, the microhardness of Ni-P-50 mL/L TiO_2/Ni-P coating was decreased to ~565 HV_{50}.

In general, the improvement of nanocomposite coatings hardness could be attributed to several factors including dispersion strengthening, grain refinement and lattice distortion, etc. As all the coatings present a similar amorphous structure, the improvement of duplex Ni-P-TiO_2/Ni-P nanocomposite coatings hardness could be mainly ascribed to the highly dispersion of TiO_2 nanoparticles. The highly dispersed TiO_2 nanoparticles, which well distributed in the grain boundary areas, can hinder the grain growth and lead to a grain refinement strengthening effect, as convinced by Fig. 3. Moreover, these uniform distributed TiO_2 nanoparticles can also lead to a significant effect of second phase dispersion strengthening. However, large amounts of sol addition resulted in excessive in-situ formed TiO_2 nanoparticles and caused a significant agglomeration in the electrolyte. The agglomerated TiO_2 nanoparticles were incorporated into the growing coating matrix and caused a loose and porous structure nearby as shown in Fig. 4(d), thereby impacting the dispersion strengthening effect and leading to a deterioration of the mechanical property.

3.3.2 Wear property

The average friction coefficients of Ni-P coating and duplex Ni-P-TiO_2/Ni-P nanocomposite coatings are shown in Fig. 6. Compared with ~0.55 (average friction coefficient) of single Ni-P coating, the average friction coefficient of duplex Ni-P/Ni-P coating is ~0.35, which decreased by ~36%. This is due to the levelling effect caused by duplex coating. After adding TiO_2 sol, the friction coefficient of duplex coating was further reduced to ~0.27, which could be explained by the grain refinement caused by highly dispersed TiO_2 nanoparticles, as convinced in Fig. 3(b). However, when the TiO_2 sol addition is 50 mL/L, the friction coefficient increased to ~0.53, which could be attributed to the porous structure caused by the agglomeration of TiO_2 nanoparticles.

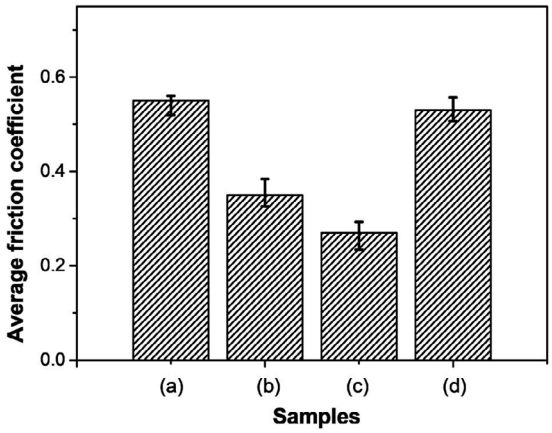

Figure 6. Average friction coefficient of (a) Ni-P; (b) Ni-P/Ni-P; (c) Ni-P-12.5mL/L TiO_2/Ni-P; (d) Ni-P-50mL/L TiO_2/Ni-P.

Fig. 7 shows the wear track images of Ni-P coating and duplex Ni-P-TiO_2/Ni-P nanocomposite coatings. The single Ni-P coating has the worst wear property with a wear track width of ~314μm. There are obvious plowing lines and some large wear debris on the worn surface. The main wear mechanism of Ni-P coating is adhesive wear, which is the most common wear mechanism for electroplated Ni-P, Ni-B and Ni-Co coatings. The corresponding wear track width of duplex Ni-P/Ni-P coating decreased to ~68 μm, probably due to the higher hardness and lower friction coefficient of coating.

When proper TiO_2 sol (12.5 mL/L) was added, the worn area decreased and the plough lines became shallower and more uniform. The corresponding wear track width further decreased to ~28 μm. This is probably caused by the incorporation of nanoparticle reinforcement. The dispersion of TiO_2 nanoparticles enhanced the microhardness and also reduced the real contact between the coating and abrasive surface. On the other hand, TiO_2 nanoparticles could act as solid-lubricant to enhance the wear performance during sliding process. However, excessive TiO_2 sol addition led to a notable deterioration of wear property. The wear track width of duplex Ni-P-50mL/L TiO_2/Ni-P was increased to ~306μm. The microhardness of Ni-P-50 mL/L TiO_2/Ni-P coating was slightly higher than ~545 HV_{50} of the Ni-P/Ni-P coating. However, their wear performances are obviously different.

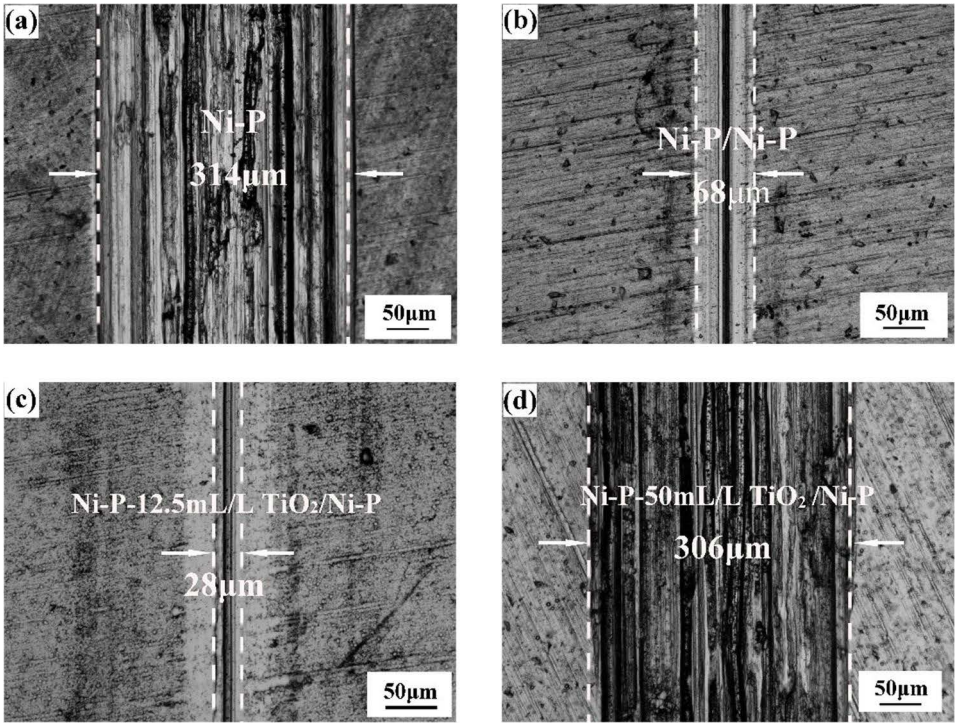

Figure 7. Wear track width of (a) Ni-P; (b) Ni-P/Ni-P; (c) Ni-P-12.5mL/L TiO_2/Ni-P and (d) Ni-P-50mL/L TiO_2/Ni-P coatings.

The wear track width was ~306 μm and ~68 μm, respectively. The reason could be interpreted by the porous structure and increased friction coefficient. As shown in Fig. 4, larger agglomeration areas and even smaller voids can be clearly observed in the outer layer matrix. In addition, Ni-P-50 mL/L TiO_2/Ni-P coating has a higher friction coefficient (~0.53) than Ni-P/Ni-P coating (~0.35). A further investigation which mainly focuses on the wear performance of sol-enhanced Ni-P-TiO_2/Ni-P coatings will be conducted to clarify the related mechanisms.

3.4 Corrosion resistance

3.4.1 Tafel plots

The corrosion resistance of the coatings was studied by electrochemical methods. Fig. 8 presents the potentiodynamic polarization curves of Ni-P and duplex Ni-P-TiO_2/Ni-P coatings in the 3.5 wt.% NaCl solution. The values of i_{corr}, E_{corr}, R_p and corrosion rate were obtained from the potentiodynamic polarization curves and summarized in Table 2.

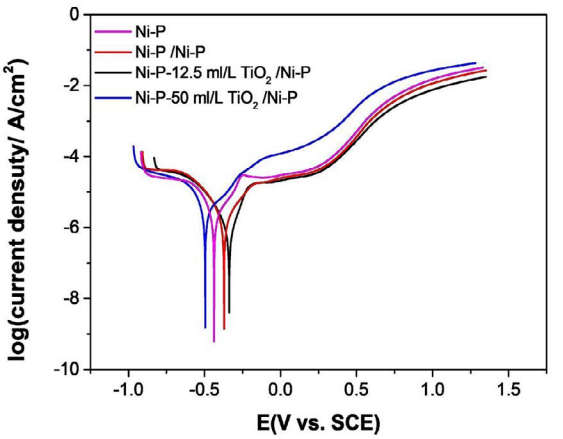

Figure 8. Potentiodynamic polarization curves of Ni-P coating and duplex Ni-P-TiO_2/Ni-P coatings.

According to Table 2, The value of E_{corr} and i_{corr} for high P Ni-P coating is -0.437V and 4.17μA/cm^2, respectively, exhibiting a typical value of Ni-P coating.

Table 2. Potentiodynamic polarization parameters for Ni-P coating and duplex Ni-P-TiO_2/Ni-P coatings

Sample	E_{corr}(V/SCE)	R_p(Ω cm^2)	i_{corr}(μA/cm^2)	Corrosion rate (mm/a)
Ni-P	-0.437	13.05	4.17	0.043
Ni-P/Ni-P	-0.372	17.39	2.92	0.030
Ni-P-12.5mL/LTiO$_2$/ Ni-P	-0.338	26.45	1.37	0.014
Ni-P-50mL/LTiO$_2$/Ni-P	-0.496	9.20	4.67	0.051

When another low-phosphorus Ni-P layer was electroplated onto the high P Ni-P coating surface, the corrosion resistance of duplex coating increased, evidenced by the increased E_{corr} of ~-0.372 V and decreased i_{corr} of 2.92 μA/cm^2.

After adding TiO_2 sol, the value of E_{corr} and i_{corr} for duplex coatings varied significantly. The duplex Ni-P-12.5 mL/L TiO_2/Ni-P coating has the most positive E_{corr} of ~-0.338 V and the lowest i_{corr} of 1.37 μA/cm^2, indicating an observably enhanced corrosion performance. Correspondingly, the duplex Ni-P-50 mL/L TiO_2/Ni-P coating shows the most negative E_{corr} of ~-0.496 V and the highest i_{corr} of 4.67 μA/cm^2, presenting a remarkably deteriorated corrosion performance which is even worse than single Ni-P coating.

For a single layer of Ni-P coating, corrosion usually develops vertically from the coating surface to the substrate matrix through the unavoidable pores of the coating. A micro circuit can form between the coating and underneath substrate. After adopting dual coating, the corrosion of duplex Ni-P/Ni-P coating usually develops horizontally. On the other hand, the outer layer of low phosphorus Ni-P coating has a relatively low corrosion potential, while the inner layer of high phosphorus Ni-P coating presents a relatively high corrosion potential. Due to the corrosion potential difference of two layers, the low phosphorus Ni-P coating layer will act as the sacrificial anode while the high phosphorus Ni-P coating layer will act as the cathode [3], explaining the corrosion resistance of duplex Ni-P/Ni-P coating is better than single Ni-P coating. After adding proper amount of TiO_2 sol, the corrosion resistance of duplex coatings becomes better. This can be explained as the incorporation of TiO_2 can reduce the crevices, gaps and micron holes in the coating matrix. However, when excessive TiO_2 sol were added, the corrosion resistance of duplex coating decreased. The reason can be mainly attributed to the porous structure of the coating caused by the TiO_2 nanoparticles agglomeration.

3.4.2 EIS

It is well known that the EIS is a powerful electrochemical technique for characterizing the corrosion behavior of coatings[19-21]. Fig. 9 presents the EIS spectra of Nyquist plots for the Ni-P coating and duplex Ni-P-TiO_2/Ni-P coatings immersed in 3.5 wt.% NaCl solutions. Single capacitive impedance loops with different diameters were observed on the Nyquist plots of Ni-P, Ni-P/Ni-P and Ni-P-12.5mL/L TiO_2/Ni-P coatings in the investigated frequency regions. In addition to the semicircle, another curve can be observed on the Nyquist plots for duplex Ni-P-50mL/L TiO_2/Ni-P coating, as shown in Fig. 9. It is indicated that when excessive quantities of TiO_2 sol (50mL/L) was added to the plating solution, the electrochemical impedance is not only caused by the charge transfer process but also by the diffusion process.

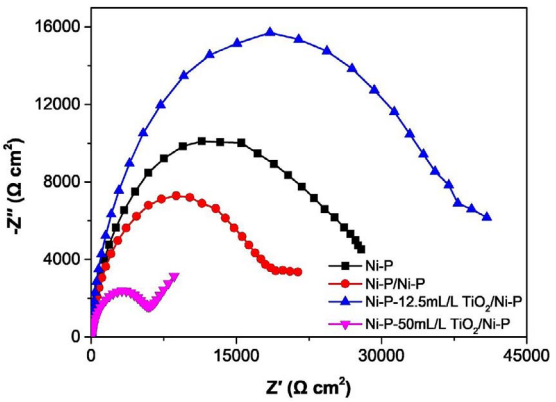

Figure 9. Nyquist plots for Ni-P and duplex Ni-P-TiO_2/Ni-P coatings.

In the impedance measurement, the diameter of the semi-circle is related to the polarization resistance of the surface. Ni-P coating has the smallest diameter. The diameter of capacitive loop in Nyquist plot was increased when depositing another Ni-P layer as the outer layer. After incorporating TiO_2 into the Ni-P outer layer, the diameter of capacitive loop increased at first, then decreased, which is consistent with the trend of the tafel plot variation.

The Bode plots are shown in Fig.10. Based on the Bode plots, it can be inferred that the Nyquist semicircles should have two time constants. For the Fig. 10(b), the value of |Z| for Ni-P/Ni-P and Ni-P-12.5mL/L TiO_2/Ni-P coatings at a fixed frequency of 0.01Hz, which usually corresponds to the polarization resistance of the duplex coatings is much larger than the single Ni-P coating[22]. This can be confirmed that the corrosion resistance of Ni-P coating in the NaCl solution is lower than that of duplex Ni-P/Ni-P and Ni-P-12.5mL/L TiO_2/Ni-P coatings. The value of |Z| for Ni-P-50mL/L TiO_2/Ni-P coatings at a fixed frequency of 0.01Hz is obviously lower than the other three coatings, demonstrating the worst corrosion resistance.

Different models have been proposed for interpreting impedance spectra on Ni-P based coatings [23,24]. The impedance results of Ni-P, Ni-P/Ni-P and Ni-P-12.5 mL/L TiO_2/Ni-P coatings can be analyzed based on the equivalent circuit depicted in Fig. 11(a), while the result of Ni-P-50 mL/L TiO_2/Ni-P coating can be interpreted by the equivalent circuit shown in Fig. 11(b).

In the proposed model as shown in Fig. 11(a), R_s represents the solution resistance, R_{ct} refers to the charge transfer resistance, R_1 symbolizes the pore resistance, and CPE represents the constant phase element. Correspondingly, the suggested model as shown in Fig. 11(b), R_s represents the solution resistance, R_{ct} refers to the charge transfer resistance, CPE_1 symbolizes a constant phase element and W refers to a Warburg diffusion impedance.

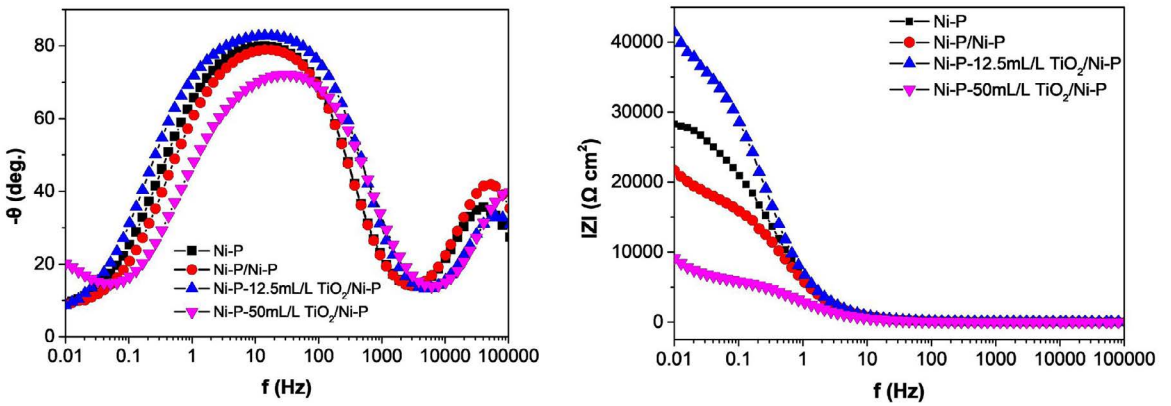

Figure 10. Bode plots for Ni-P coating and duplex Ni-P-TiO_2/Ni-P coatings. (a) The relationship between frequency and phase angle; (b) the relationship between frequency and absolute mode.

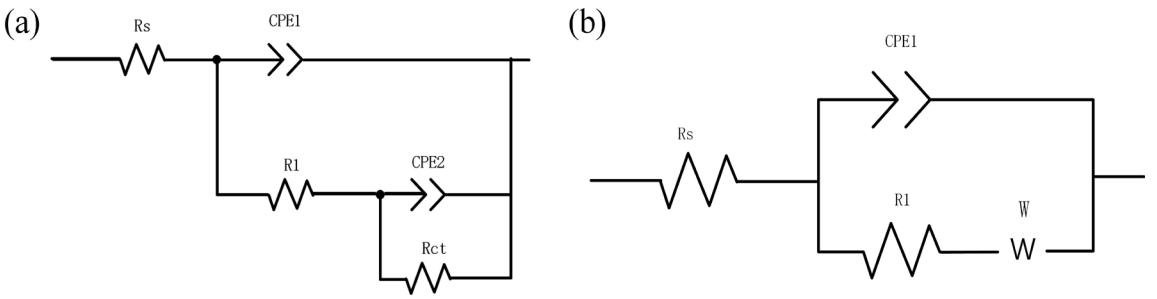

Figure 11. Equivalent electrical circuits of (a) Ni-P, Ni-P/Ni-P and Ni-P-12.5mL/L TiO_2/Ni-P coatings, (b) duplex Ni-P-50mL/L TiO_2/Ni-P coatings.

Table 3 lists the fitting parameters based on the equivalent circuits in Fig. 11. For the studied coatings, the polarization resistance ® can be computed as $R=-R_1+R_{ct}$ [25]. The R of Ni-P coating was higher than that of the duplex Ni-P/Ni-P coating, indicating the better corrosion resistance of the duplex coating, which is consistent with previous results. Notably, adding the appropriate amount of TiO_2 sol to the plating solution increased the value of R to 4.20×10^4 Ω cm^2. It can be concluded that the presence of TiO_2 reduced the number of defects in the coating contribution for the increased pore resistance(R_1). Furthermore, the presence of oxide particles(TiO_2) in the duplex Ni-P/Ni-P matrix may have a corrosion inhibiting effect, stabilizing the corrosion products and rendering them more protective. However, when excessive amount of TiO_2 sol (50mL/L) was added to the plating solution, the R (R_{ct}) of duplex Ni-P-50mL/L TiO_2/Ni-P coatings decreased to 0.56×10^4 Ω cm^2, leading to a decline in corrosion resistance. The decreased resistance values account for the increased corrosion activity and accumulation of poorly protective corrosion products, introducing a diffusional behavior. On the other hand, the presence of surface defects caused by the TiO_2 nanoparticles agglomeration, such as micro cracks or nano-porosities contributed to the significant decrease in the resistance values.

Table 3. Equivalent circuit parameters for EIS results of different coatings

Sample	R_s (Ω cm^2)	$Y_{0\text{-CPE1}}$ ($\times10^{-5}$Ω^{-1}cm^{-2}s^{-n})	n_1	R_1 (Ω cm^2)	W (10^{-3}Ω cm^{2}s$^{-1/2}$)	$Y_{0\text{-CPE2}}$ ($\times10^{-5}$Ω^{-1}cm^{-2}s^{-n})	n_2	Rct ($\times10^3$Ω cm^2)	R ($\times10^3$Ω cm^2)
A	0.01	2.01	0.62	37.54	--	1.51	0.99	20.7	2.07
B	25.82	2.67	0.91	23000	--	48.9	0.77	7.70	3.07
C	16.54	2.46	0.93	34200	--	63.6	0.91	7.80	4.20
D	12.84	5.30	0.85	--	1.09	--	--	5.64	0.56

Note: Sample A is the single Ni-P coating, Sample B is the duplex Ni-P/Ni-P coating, Sample C is the Ni-P-12.5 mL/L TiO2/Ni-P coating, Sample D is the Ni-P-50 mL/L TiO_2/Ni-P coating

4. Conclusions

Double-layered Ni-P-TiO_2/Ni-P coatings with different P contents have been successfully fabricated on the brass substrate by using a simple electrodeposition process. The high phosphorus inner layer provides high corrosion resistance while the sol-enhanced composite outer layer provides excellent mechanical properties. The structural, morphological, mechanical and electrochemical properties of the duplex Ni-P-TiO_2/Ni-P coating were analyzed. The results showed that the hardness and the corrosion resistance of the duplex coatings were greatly improved by adding a suitable amount of TiO_2 sol. Ni-P-12.5mL/L TiO_2/Ni-P coating exhibited a significantly enhanced mechanical property and improved corrosion resistance compared with other coatings. Further research will be focused on the development of its future applications in industry.

5. Acknowledgements

This research was supported by National Natural Science Foundation of China (51601073), Jiangsu Distinguished Professor Project (1064901601), Start research fund of Jiangsu University of Science and Technology (1624821607-5), Project of Jiangsu Provincial Six Talent Peaks (2018 XCL-028) and Jiangsu Postgraduate Research Innovation Project.

6. References

1. Jeong DH, Erb U, Aust KT, Palumbo G. The relationship between hardness and abrasive wear resistance of electrodeposited nanocrystalline Ni-P coatings. *Scripta Materialia*. 2003;48(8):1067-1072.

2. Zhou XW, Wu F, Ouyang C. Electroless Ni-P alloys on nanoporous ATO surface of Ti Substrate. *Journal of Materials Science*. 2018;53(4):2812-2829.

3. Dai DH, Zhou KZ, Yuan ZH. *Science of surface technology of modern materials*. Beijing: Metallurgical Industry Press; 2004. p. 10-14.

4. Gu CD, Lian JS, Li GY, Niu LY, Jiang ZH. High corrosion-resistant Ni-P/Ni/Ni-P multilayer coatings on steel. *Surface and Coatings Technology*. 2005;197(1):61-67.

5. Sahoo P, Das SK. Tribology of electroless nickel coatings - A review. *Materials & Design*. 2011;32(4):1760-1775.

6. Zhang WH, Cao D, Qiao YX, Wang YX, Li X, Gao W. Preparation and property of duplex Ni-P-TiO2/Ni nanocomposite coatings. *International Journal of Modern Physics B*. 2019;33:1940019.

7. Tohidi A, Monirvaghefi SM, Hadipour A. Properties of Electroless Ni-B and Ni-P/Ni-B Coatings Formed on Stainless Steel. *Transactions of the Indian Institute of Metals*. 2017;70(7):1735-1742.

8. Georgiza E, Novakovic J, Vassiliou P. Characterization and corrosion resistance of duplex electroless Ni-P composite coatings on magnesium alloy. *Surface and Coatings Technology*. 2013;232:432-439.

9. Wang YX, Tay SL, Zhou XW, Yao CZ, Gao W, Cheng G. Influence of Bi addition on the property of Ag-Bi nano-composite coatings. *Surface and Coatings Technology*. 2018;349:217-223.

10. Wang YX, Cheng G, Tay SL, Guo YX, Sun X, Gao W. Effects of Bi Addition on the Microstructure and Mechanical Properties of Nanocrystalline Ag Coatings. *Materials (Basel)*. 2017;10(8). pii: E932.

11. Zhou XW, Ouyang C. Anodized porous titanium coated with Ni-CeO2 deposits for enhancing surface toughness and wear resistance. *Applied Surface Science*. 2017;405:476-488.

12. Sheng YY, Yang J, Wang F, Liu LC, Liu H, Yan C, et al. Sol-gel synthesized hexagonal boron nitride/titania nanocomposites with enhanced photocatalytic activity. *Applied Surface Science*. 2019;465:154-163.

13. Wang YX, Shu X, Wei SH, Liu CM, Gao W, Shakoor RA, et al. Duplex Ni-P-ZrO2/Ni-P electroless coating on stainless steel. *Journal of Alloys and Compounds*. 2015;630:189-194.

14. Shu X, Wang YX, Liu C, Alijaafari A, Gao W. Double-layered Ni-P/Ni-P-ZrO2 electroless coatings on AZ31 magnesium alloy with improved corrosion resistance. *Surface and Coatings Technology*. 2015;261:161-166.

15. Wang YX, Tay SL, Wei SG, Xiong C, Gao W, Shakoor RA, et al. Microstructure and properties of sol-enhanced Ni-Co-TiO2 nanocomposite coatings on mild steel. *Journal of Alloys and Compounds*. 2015;649:222-228.

16. Chen WW, Gao W, inventors. *Plating or coating method for producing metal-ceramic coating on a substrate*. New Zealand Patent NZ 578038. 2009 Jun 29.

17. Yang YJ, Chen WW, Zhou CW, Xu HB, Gao W. Fabrication and characterization of electroless Ni-P-ZrO2 nano-composite coatings. *Applied Nanoscience*. 2011;1(1):19-26.

18. Gao WD, Cao D, Jin YX, Zhou XW, Cheng G, Wang YX. Microstructure and properties of Cu-Sn-Zn-TiO2 Nano-composite coatings on mild steel. *Surface and Coatings Technology*. 2018;350:801-806.

19. Ma C, Wu F, Ning Y, Xia F, Liu Y. Effect of heat treatment on structures and corrosion characteristics of electroless Ni-P-SiC nanocomposite coatings. *Ceramics International*. 2014;40(7 Pt A):9279-9284.

20. Walkner S, Hassel AW. Combined chemical and EIS study of the reaction of zinc coatings under alkaline conditions. *Electrochimica Acta*. 2014;131:130-136.

21. Madram AR, Pourfarzad H, Zare HR. Study of the corrosion behavior of electrodeposited Ni-P and Ni-P-C nanocomposite coatings in 1 M NaOH. *Electrochimica Acta*. 2012;85:263-267.

22. Luo H, Leitch M, Behnamian Y, Ma YS, Zeng HB, Luo JL. Development of electroless Ni-P/nano-WC composite coatings and investigation on its properties. *Surface and Coatings Technology*. 2015;277:99-106.

23. Balaraju JN, Selvi VE, Rajam KS. Electrochemical behavior of low phosphorus electroless Ni-P-Si3N4 composite coatings. *Materials Chemistry and Physics*. 2010;120(2-3):546-551.

24. Chen MA, Cheng N, Ou YC, Li JM. Corrosion performance of electroless Ni-P on polymer coating of MAO coated AZ31 magnesium alloy. *Surface and Coatings Technology*. 2013;232:726-733.

25. Ashassi-sorkhabi H, Es'haghi M. Corrosion resistance enhancement of electroless Ni-P coating by incorporation of ultrasonically dispersed diamond nanoparticles. *Corrosion Science*. 2013;77:185-193.